Rheological Behavior of Noncompatibilized and Compatibilized PP/PET Blends with SEBS-*g*-MA

Z. Kordjazi, N. Golshan Ebrahimi

Department of Chemical Engineering, Faculty of Engineering, Polymer Group, Tarbiat Modares University, Tehran 14115-143, Iran

Received 26 November 2008; accepted 6 September 2009
DOI 10.1002/app.31471
Published online 1 December 2009 in Wiley InterScience (www.interscience.wiley.com).

ABSTRACT: The rheological behaviors of noncompatibilized and compatibilized polypropylene/polyethylene terephthalate blends (80/20) in relation with their morphology were studied at two constant levels using maleic anhydride-modified styrene-ethylene-butylene-styrene polymer. By scanning electron microscopy of cryofractured surfaces, the morphology of the blends was examined after etching. The frequency sweep and step strain experiments were carried out for the blends. The frequency sweep results indicated that increasing the compatibilizer causes behavioral changes of the rheological properties, which could be related to the aggregation of the dispersed particles with rubbery shell. Also, the frequency sweep and step strain experiments in linear region, after cessation of simple steady shear flow with various preshear rates (higher shear stress values than G'_p), were done on compatibilized blend. The results showed that the morphology characteristics, defined by the aggregation of the dispersed particles based on rheological experimental data, were destroyed and replaced by an alignment in the flow direction for present imposed shear rates. © 2009 Wiley Periodicals, Inc. J Appl Polym Sci 116: 441–448, 2010

Key words: rheology; morphology; immiscible blends; polypropylene; polyethylene terephthalate

INTRODUCTION

Blending of polymers is a beneficial and cheap way of developing new materials. However, the polymers being blended are often thermodynamically immiscible. Droplet/matrix, fibrillar, lamellar, or cocontinuous morphologies can occur during blending. Each of these resulting morphologies depends on the composition of the blend components, processing conditions, or nature of the polymers.[1,2] Compatibilizers are added to the blends to promote mixing of incompatible polymers, which leads to reduction in the average droplet size, delay of coalescence of the dispersed phase, and decrease in interfacial tension.[3,4]

Among thermoplastic polymer blends, polypropylene/polyethylene terephthalate (PP/PET) blends have some advantages over the pure components. In addition, potential compatibilizers are reported to improve compatibility. For example, the effect of a triblock copolymer on the morphology and interfacial tension of PP/PET blends is studied, and the interfacial tension of PP/PET blend containing modifier was measured by breaking thread method.[5] Also, the compatibilizing efficiency for PP/PET blends with various compatibilizers is compared.[6] However, it should be mentioned that the effect of compatibilizers on the rheological properties of PP/PET blends was not studied.

The first attempt of viscoelastic approach was proposed by Froehlich and Sack on the rheological behavior of a suspension of elastic and slightly deformable spheres in a Newtonian fluid, which showed time-dependent elastic recovery when subjected to external macroscopic stresses. Oldroyd used the Froehlich and Sack approach for complex viscosity of emulsions of Newtonian liquids in time-dependent flows and developed the effect of interfacial tension on viscoelastic treatments. Oldroyd's theory was extended by Palierne.[7] He developed a general model, which could predict the linear viscoelastic behavior of polymer emulsions.[8] However, the Palierne model was originally developed for dilute concentration of dispersed phase. Although the Palierne model predicts the dynamic modulus of multiphase polymer melts, it fails in prediction of the secondary plateau of concentrated blends with no deformable particles. Several authors have reported this plateau in rubber-toughened polymers.[9] Also, the blends with rubbery dispersed phase have been studied under flow condition with viscosity and postextrusion swell. The results showed that the final properties of rubber-toughened thermoplastic polymers depend on the state of the rubber particles in the thermoplastic matrix, which is itself controlled by the deformation history

Correspondence to: N. G. Ebrahimi (ebrahimn@modares.ac.ir).

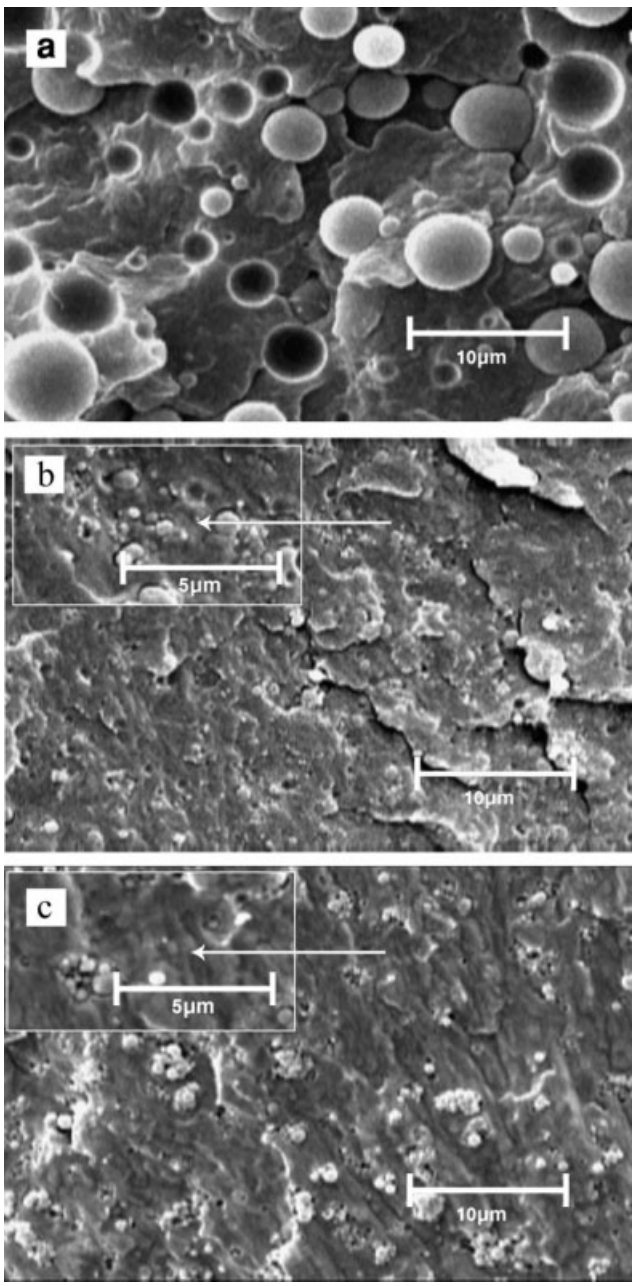

Figure 1 The SEM micrograph of noncomptatibilized and compatibilized blends with SEBS-*g*-MA: (a) 80-20-0, (b) 80-20-2.5, and (c) 80-20-5.

(rheology) involved during the mechanical melt blending.[10]

In this work, the correlation between rheological properties and morphology of the compatibilized and noncompatibilized PP/PET blends with maleic anhydride-modified styrene-ethylene-butylene-styrene (SEBS-*g*-MA) as a rubbery compatibilizer is investigated. The frequency sweep experiments were carried out for the blends in addition to the step strain experiments without preshear and after cessation of various simple shear flows on compatibilized blend.

EXPERIMENTAL

Materials

The blends investigated in this study used PP as the matrix and PET as the dispersed phase. The PP was obtained from Arak Petrochemical Company (V30S grade) (Iran) with MFR 18 g/10 min (230°C/2.16 kg), and the PET (bottle grade) was purchased from Sabic Company (Saudi Arabia). Styrene-ethylene-butylene-styrene linear triblock copolymer grafted with 2% maleic anhydride was supplied by Shell under the name of Kraton FG1901X containing 30% polystyrene. Irganox 1010 (Ciba-Geigy) was used as antioxidant in all polyblends with constant amount of 0.2 wt %.

Blend preparation

Before blend preparation, PP and PET were dried for 24 h in vacuum oven (PET at 110°C and PP at 60°C). The PP/PET blends, having different compatibilizers, were prepared in a Brabender internal mixer at 265°C with the rotor speed of 60 rpm for 10 min. The compatibilizer SEBS-*g*-MA of 2.5 and 5 wt % were used to compatibilize the PP/PET blend bearing 20 wt % PET.

Rheological measurements

The rheological measurements were performed using UDS 200 rheometer (made by Paar Physica) at 265°C with disk-type parallel plates (plate diameter of 25 mm and 1 mm gap). The frequency sweep tests were carried out in linear viscoelastic region. A fresh sample was used in each test, which had been held into the shear cell at a temperature of 265°C for 10 min (after loading and trimming excess sample) to allow morphology relaxation and to eradicate the sample history.

Sample preparation for morphological characterization

The morphology of cryofractured (in liquid nitrogen) surfaces, after coating with a thin layer of gold, was studied with scanning electron microscopy (SEM) (Philips model XL 300 microscope). It should be noted that the fractured surfaces, before coating with gold, were etched by cyclohexane for 24 h at room temperature to remove the rubber phase. The morphology of quenched samples at room temperature

TABLE I
The Number- and Volume-Average Radii of Blends

Blend	$\overline{R}_n(\mu m)$	$\overline{R}_v(\mu m)$
80-20-0	1.43	2.03
80-20-2.5	0.24	0.32
80-20-5	0.19	0.25

TABLE II
The Surface Tension of Polymers at 265°C

Polymer	γ(mN/m)	γ^p(mN/m)	γ^d(mN/m)
PP	15.80	0.31	15.52
PET	28.67	6.33	22.34
SEBS-*g*-MA	22.63	0.36	22.27

for rheological tests was found to be similar to quenched blends in liquid nitrogen at 265°C.

RESULTS AND DISCUSSION

Blend morphology

Figure 1 shows the SEM micrographs of noncompatibilized and compatibilized PP/PET blends with SEBS-*g*-MA. We use the number-average $\overline{R}_n$ and the volume-average $\overline{R}_v$ radii of droplets for the quantitative comparison of morphologies:

$$\overline{R}_n = \frac{\sum_{i=1}^{\infty} n_i R_i}{\sum_{i=1}^{\infty} n_i} \tag{1a}$$

$$\overline{R}_v = \frac{\sum_{i=1}^{\infty} n_i R_i^4}{\sum_{i=1}^{\infty} n_i R_i^3}. \tag{1b}$$

The results of the surface analysis of at least 200 particles with desired accuracy are shown in Table I. It can be seen that by adding compatibilizer to the blend and with increasing the amount of compatibilizer, the average radius of the dispersed phase has decreased. This is the result of reaction MA grafted on SEBS with the carboxylic acid end groups of PET and also an affinity between the SEBS and polyolefin. On the other hand, the presence of PS blocks prevents copolymer migration and loss into the polyolefin phase.[6]

As seen in Figure 1, the compatibilized blend has core-shell-type morphology in which the PET core encapsulated by the SEBS-*g*-MA. The morphological observation showed that in this concentration, the PET particles with elastomeric shell are dispersed in a three-dimensional (3D) agglomerated structure.

TABLE III
Calculated Spreading Coefficients of the Compatibilized Blend with SEBS-*g*-MA at 265°C

Blend	1	2	3	λ_{13}	λ_{31}
PP/PET/SEBS-*g*-MA	PET	PP	SEBS-*g*-MA	−10.8	0.145

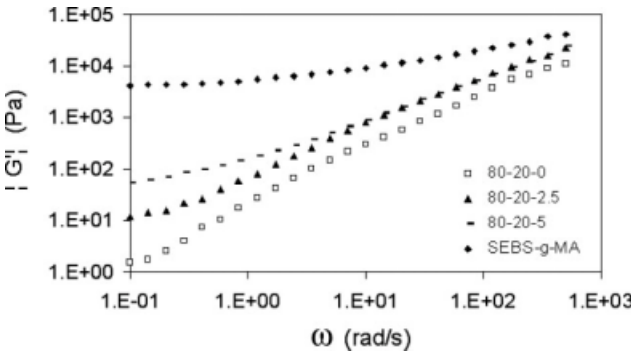

Figure 2 Dynamic storage moduli of noncompatibilized and compatibilized blends with SEBS-*g*-MA.

Hobbs et al.[11] and Luzinov et al.[12] used Harkin's spreading coefficient concept to explain morphologies of ternary blends. For a ternary system with components 1, 2, and 3, the spreading coefficient can be predicted by the following equation:

$$\lambda_{31} = \gamma_{12} - \gamma_{23} - \gamma_{31}, \tag{2}$$

where γ_{12}, γ_{23}, and γ_{13} are the interfacial tensions for each component pair (index 2 refers to the matrix). For component 3 to spread over dispersed component 1, γ_{31} must be positive. Similar treatment gives the spreading coefficient of the component 1 on the component 3:

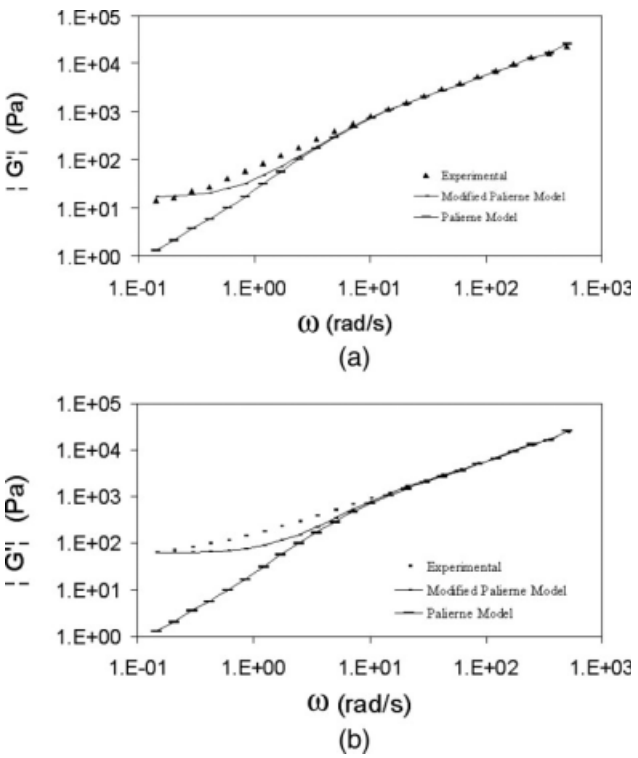

Figure 3 Comparison between experimental and predicted results from Palierne model and modified model for compatibilized blends with SEBS-*g*-MA: (a) 80-20-2.5 and (b) 80-20-5.

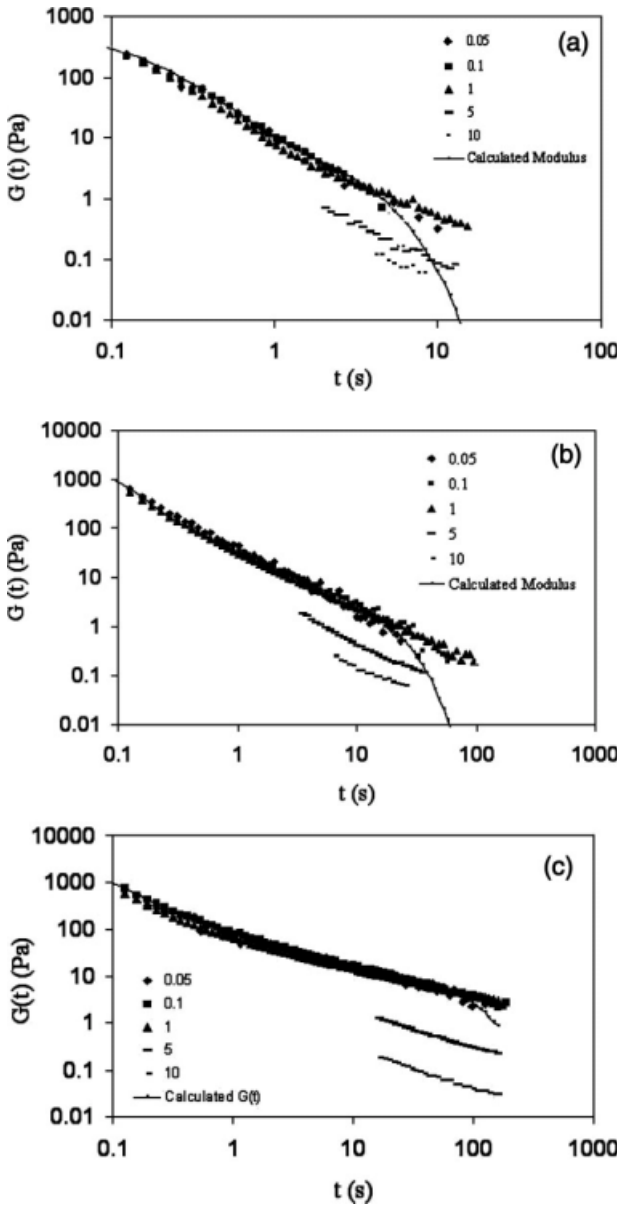

Figure 4 The relaxation moduli for noncompatibilized and compatibilized blends with SEBS-*g*-MA: (a) 80-20-0, (b) 80-20-2.5, and (c) 80-20-5.

$$\lambda_{13} = \gamma_{32} - \gamma_{21} - \gamma_{13}. \quad (3)$$

A positive value of λ_{13} will lead to a core-shell morphology in which 3 to be encapsulated by 1. If both λ_{13} and λ_{31} are negative, the 1 and 3 components will remain separate. Interfacial tension between polymers can be calculated using the harmonic mean equation:[13]

$$\gamma_{12} = \gamma_1 + \gamma_2 - \frac{4\gamma_1^d\gamma_2^d}{\gamma_1^d + \gamma_2^d} - \frac{4\gamma_1^p\gamma_2^p}{\gamma_1^p + \gamma_2^p}, \quad (4)$$

where γ_1, γ_2, γ^p, and γ^d denote the γ values of each phase and their polar and dispersive components, respectively. Values of calculated surface tension for PP, PET, and SEBS-*g*-MA are listed in Table II, and the spreading coefficients at 265°C are listed in Table III. As seen, λ_{13} is negative and λ_{31} is positive. Therefore, the results predict that for PP/SEBS-*g*-MA/PET blend, the PET will be encapsulated by the rubber phase (SEBS-*g*-MA), which is consistent with our morphological observations.

TABLE IV
The Parameters of Generalized Maxwell Model for Noncompatibilized and Compatibilized Blends with SEBS-*g*-MA [T4: a 80-20-0; b 80-20-2.5; c 80-20-5]

	i	G_i	τ_i
(a) 80-20-0	1	11,000	0.001
	2	2000	0.01
	3	500	0.1
	4	110	0.3
	5	10	2
(b) 80-20-2.5	1	12,981	0.004
	2	4001	0.06
	3	201	0.3
	4	30	1.5
	5	8	10
(c) 80-20-5	1	13,001	0.004
	2	2400	0.06
	3	370	0.3
	4	72	2.6
	5	16	45

Blend rheology

Frequency sweep

In 1990, Palierne published a general model for the linear rheology of viscoelastic emulsions.[8] The Palierne model for the linear rheology of viscoelastic emulsions can predict the melt linear viscoelastic properties of polymer blends. In case of an emulsion of two viscoelastic phases, with narrow distribution particle size and constant interfacial tension, Palierne model simplified to:

$$G_b^*(\omega) = G_m^*(\omega)\frac{1 + 3\Phi H(\omega)}{1 - 2\Phi H(\omega)}, \quad (5)$$

TABLE V
Calculated Zero Shear Viscosity for Noncompatibilized and Compatibilized Blends with SEBS-*g*-MA

Blend	η_0 (Pa s)
80-20-0	112.2
80-20-2.5	482.3
80-20-5	1259

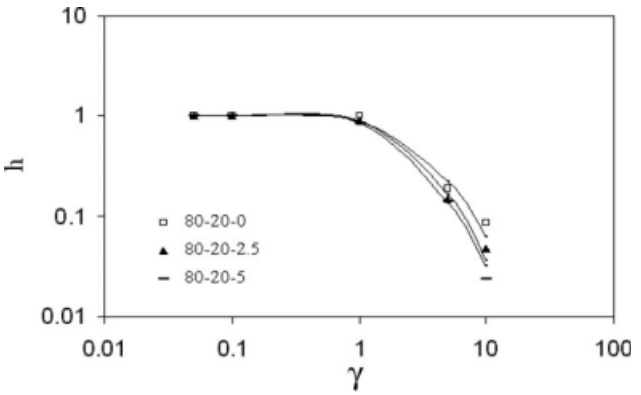

Figure 5 The log–log plot of damping function versus strain for noncompatibilized and compatibilized blend with SEBS-*g*-MA (The curves are the best fitting with Soskey–Winter for each data series with parameters shown in Table VI).

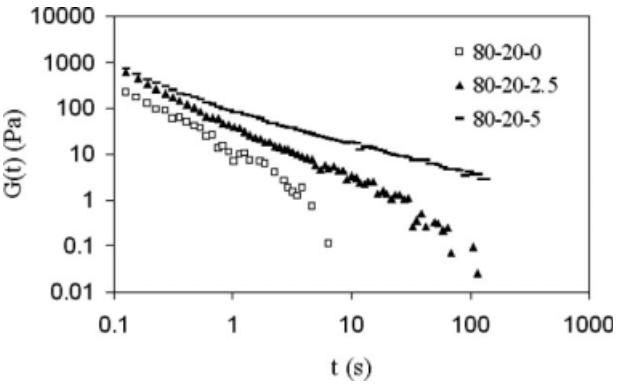

Figure 6 The relaxation moduli for noncompatibilized and compatibilized blends with SEBS-*g*-MA at $\gamma = 0.1$.

where

$$H(\omega) = \frac{4(\alpha/R)[2G_m^*(\omega) + 5G_d^*(\omega)] + [G_d^*(\omega) - G_m^*(\omega)][16G_m^*(\omega) + 19G_d^*(\omega)]}{40(\alpha/R)[G_m^*(\omega) + G_d^*(\omega)] + [2G_d^*(\omega) + 3G_m^*(\omega)][16G_m^*(\omega) + 19G_d^*(\omega)]} \quad (6)$$

in which Φ is the volume fraction of droplets with radius R; G_m^*, G_d^*, and G_b^* represent complex shear moduli of the matrix, dispersed phase, and blend, respectively. α is interfacial tension and ω is the strain frequency. Figure 2 shows the dynamic storage moduli of the noncompatibilized and compatibilized blends. As seen at low frequencies, the changes in storage modulus have occurred in secondary plateau region, which increases by increasing the compatibilizer. The secondary plateau for noncompatibilized blend can be attributed to the shape relaxation (a deformed droplet has regained its spherical form). However, for compatibilized blends, it is related to the aggregation of the dispersed phase particles encapsulated with elastomeric shell. The values of this secondary plateau (G_p') were equal to 11.9 and 54.4 Pa in the blends with 2.5 and 5 phr compatibilizer, respectively.

Figure 3(a,b) shows the comparison between Palierne model predictions with the experimental storage modulus of compatibilized blends. It can be clearly seen that the Palierne model fits well to the experimental data only at high frequencies. The disagreement observed at low frequencies may be due to the aggregation of dispersed particles. Also, the discrepancy between experimental data and Palierne model prediction is increased with increasing the amount of compatibilizer. The Palierne emulsion model can be empirically modified to describe the data by simply adding a constant modulus for each composition [Fig. 3(a,b)].

TABLE VI
Soskey–Winter Parameters Used to Fitted Damping Function for Noncompatibilized and Compatibilized Blends with SEBS-*g*-MA

	Soskey–Winter	
Blend	*a*	*b*
80-20-0	0.1200	2.100
80-20-2.5	0.1132	2.3654
80-20-5	0.1644	2.2651

Step strain

The step strain experiments were done on noncompatibilized and compatibiized blends with SEBS-*g*-MA for five strains: 0.05, 0.1, 1, 5, and 10 [Fig. 4(a–c)]. In general, the relaxation modulus is a function of the strain magnitude. When the strain is very small, they are independent of the applied strain. In this work, linearity is obtained at strain below 1. In linear regime, we used a method to correlate the

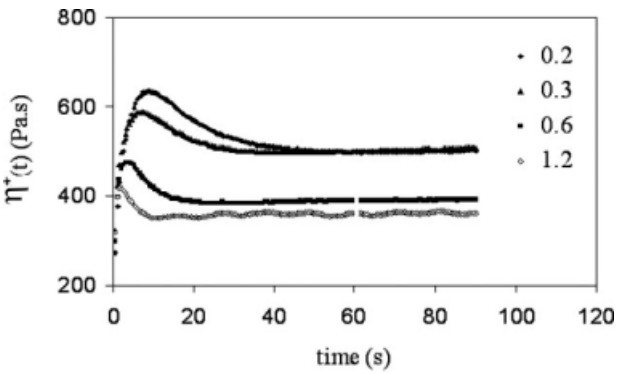

Figure 7 The stress growth coefficient for compatibilized blend with SEBS-*g*-MA (80-20-5).

TABLE VII
Steady Shear Stress Values for Compatibilized Blend with SEBS-*g*-MA (80-20-5)

Shear rate (s^{-1})	Steady shear stress (Pa)
0.2	101.2
0.3	151.8
0.6	235.8
1.2	438

relaxation modulus of the blends. A generalized Maxwell model is applied as:[14]

$$G(t) = \sum_{i=1}^{n} G_i e^{\frac{-t}{\tau_i}}, \quad (7)$$

where G_i and τ_i are the modulus and the relaxation time of ith mode, respectively. By use of a sufficient number of elements, this equation can be made to describe almost any experimental $G(t)$ behavior. The best fit values of G_i and τ_i for linear data of all blends are summarized in Table IV, and the corresponding fit is shown with solid line in Figure 4. The linear data in Table IV can be used to derive zero shear viscosity (η_0) by eq. (8).[15]

$$\eta_0 = \sum_{i=1}^{5} G_i \tau_i. \quad (8)$$

The results are shown in Table V. Because of thermal degradation at high temperatures, it was not possible to verify η_0 from terminal zone at a reference temperature of 265°C.

As the Figure 4 shows, the curves are nearly parallel at long times; hence, they should obey the time-strain separability, which could be expressed as the product of the linear modulus $G(t)$ and a damping function $h(\gamma)$:[16]

$$G(t,\gamma) = G(t)h(\gamma). \quad (9)$$

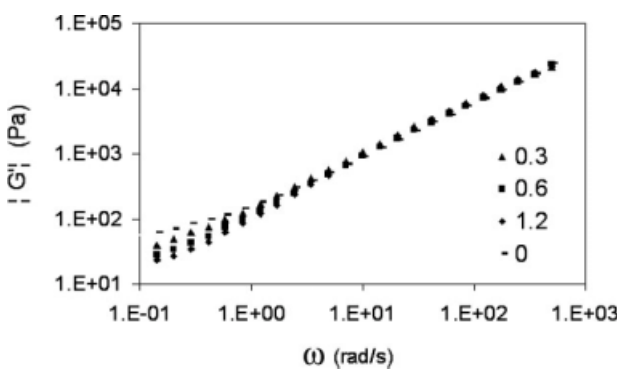

Figure 8 Dynamic storage moduli after cessation of various steady preshear rates for compatibilized blend with SEBS-*g*-MA (80-20-5).

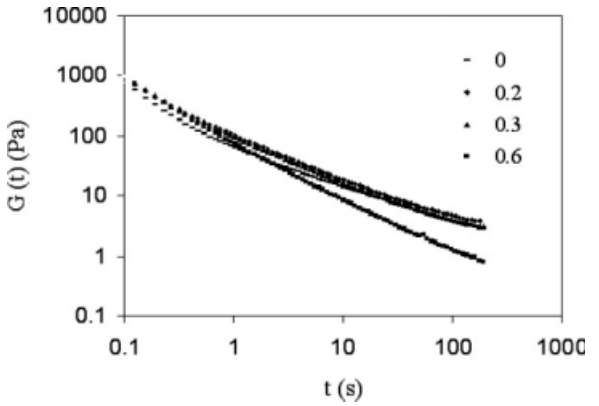

Figure 9 The relaxation moduli after cessation of various steady preshear rates for compatibilized blend with SEBS-*g*-MA (80-20-5).

Soskey and Winter proposed the following two parameters expression for the damping function[17]:

$$h(\gamma) = \frac{1}{1 + a\gamma^b}. \quad (10)$$

Figure 5 shows the values of the damping function resulting from the vertical shift on log–log plot of the relaxation moduli curves onto linear data of noncompatibilized and compatibilized blends with the prediction of Soskey–Winter (SW) equations. Table VI presents the parameters for SW equation for all of the blends. Note that the $h(\gamma)$ decreases as the strain increases. Therefore, with eq. (9) for $G(t,\gamma)$, in which the experimental damping function was fixed by the SW equation and $G(t)$ was obtained with parameters G_i and τ_i (given in Table IV for all blends), the relaxation modulus should be decreased in this case. On the other hand, as seen (Fig. 5), the damping function values decrease with increasing compatibilizer at a fixed strain. This is clearly observed for large strain amplitude $\gamma = 10$. Therefore, in result, the negative departures from linear

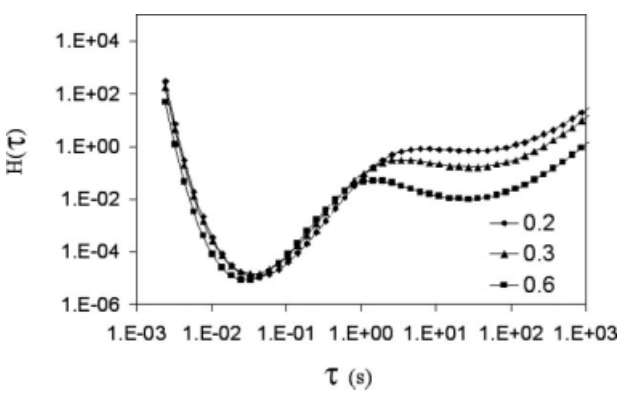

Figure 10 Relaxation time spectra after cessation of various steady preshear rates for compatibilized blend with SEBS-*g*-MA (80-20-5).

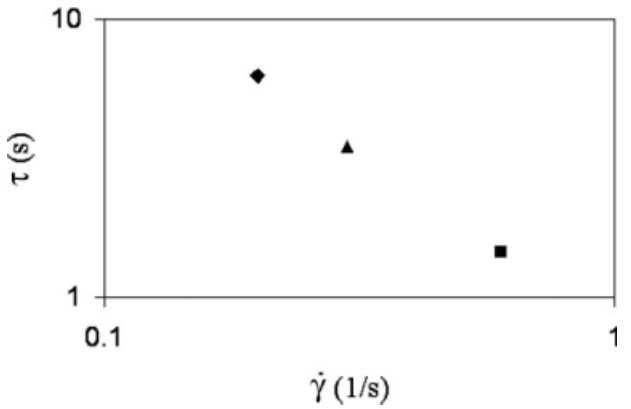

Figure 11 Relaxation time versus preshear at different rates (0.2 ◆; 0.3 ▲; 0.6 ■) for compatibilized blend with SEBS-*g*-MA (80-20-5).

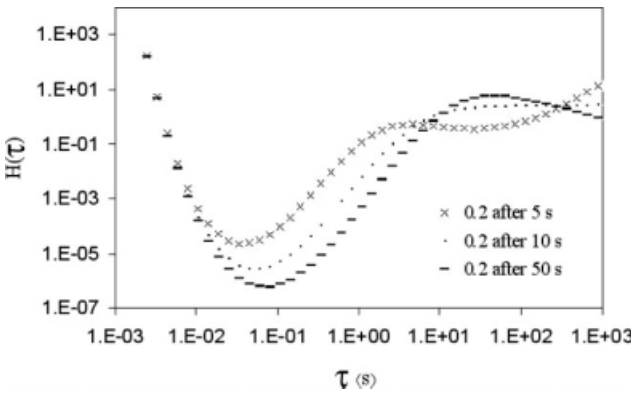

Figure 13 Relaxation time spectra after different time interval after cessation of steady shear flow of 0.2 s^{-1} for compatibilized blend with SEBS-*g*-MA (80-20-5).

behavior increase in this case. This phenomenon may be attributed to the aggregated structure of compatibilized blends, which causes to increase dependency on imposed strain.

As the experiments were performed using disk-type parallel plates, at high strain, the deformations were not homogenous through the samples and a correction should be done. Soskey and Winter proposed such a correction for this type of test as:[18]

$$G(t, \gamma_R) = \chi(\gamma_R) G_a(t, \gamma_R), \tag{11}$$

where

$$\chi(\gamma_R) = \frac{h(\gamma_R)\gamma_R^4}{4\int_0^{\gamma_R} h\gamma^3 d\gamma}. \tag{12}$$

G_a, γ_R, and h are apparent relaxation modulus, maximum strain imposed on disks circumference, and damping function, respectively. All of the data are corrected with this procedure.

In Figure 6, the relaxation moduli of noncompatibilized and compatibilized blends with SEBS-*g*-MA for $\gamma = 0.1$ are shown. The results show that by increasing the compatibilizer, almost similar behavior as oscillatory tests is observed. As seen, the storage modulus (Fig. 2) increases by increasing the compatibilizer below a frequency about 10 s^{-1}. This value may be equivalent with the lowest time, which is shown in Figure 6.

In the next section, the results of the frequency sweep and stress relaxation experiments in linear regime, after cessation of steady shear flow of various shear rates, are shown to give information about the morphology, which is generated by the previous shear flow.

Frequency sweep and step strain after cessation of simple shear flow

Figure 7 shows the stress growth coefficients of compatibilized (80-20-5) blends after different shear rates (0.2, 0.3, 0.6, and 1.2 s^{-1}). It should be mentioned that a fresh sample was used for each preshear rate,

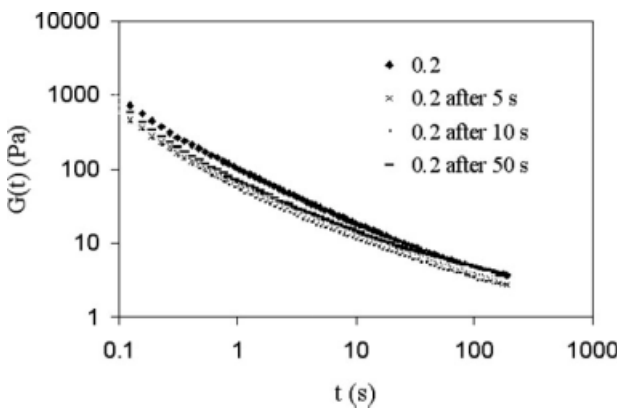

Figure 12 The relaxation moduli after different time interval after cessation of steady shear flow of 0.2 s^{-1} for compatibilized blend with SEBS-*g*-MA (80-20-5).

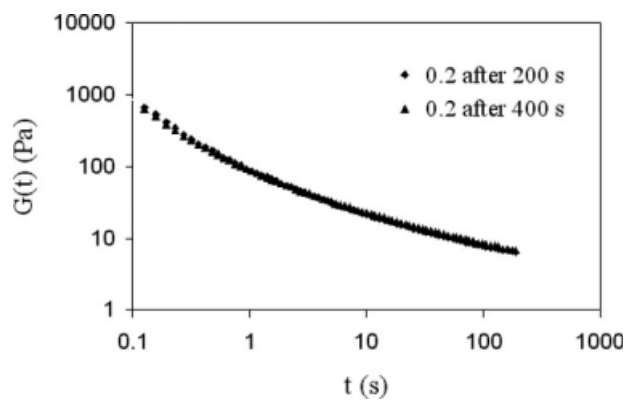

Figure 14 The relaxation moduli after long waiting times after cessation of steady shear flow of 0.2 s^{-1} for compatibilized blend with SEBS-*g*-MA (80-20-5).

and therefore, the morphology should be more distilled by increasing the shear rate. For different shear rates, an overshoot is observed at very short time, and then an equilibrium value is seen at long time. The steady shear stress values are shown in Table VII.

Frequency sweep experiments after cessation of steady shear flow (considering 90 s for all experiments) were done on compatibilized (80-20-5) blend with various preshear rates. The results are shown in Figure 8. As seen, the secondary plateau decreases by increasing the preshear rate. This plateau cannot be attributed to the shape relaxation and is due to aggregated structure formed by associating dispersed particles with rubbery shell. Therefore, this reduction in storage modulus with increase in preshear rate is probably due to destruction and orientation of the aggregated structure under preshear flow. As the shear stress values (Table VII) are higher than the G_p' value (54.4 Pa), it seems that the destruction of aggregated structure be a true prediction.

Also, the step strain experiments after cessation of steady shear flow at various shear rates were done on this compatibilized blend. The stress relaxation moduli after preshear results are shown in Figure 9. Figure 10 shows the relaxation spectra determined by relaxation modulus of Figure 9. The experimental relaxation time of the blend could be indicated from the relaxation spectra (Fig. 10) for each preshear (Fig. 11). It can be clearly seen that the relaxation time decreases by increasing the preshear rate. It means that by increasing the preshear rate, the aggregated structure is destroyed and oriented more in the flow direction as shown in frequency sweep after preshear experiments.

In the next experiment, the time interval between cessation of steady shear flow (0.2 s^{-1}) and step strain was varied (Fig. 12). The relaxation time spectra determined by relaxation modulus of Figure 12 are shown in Figure 13. It can be clearly seen that the relaxation time increases by increasing time interval (5, 10, and 50 s). Therefore, the oriented structure should be recovered. Also, after long waiting time, the relaxation curves become almost identical (Fig. 14). These results are consistent with our predictions about recovery of the oriented structure. To confirm this assumption, morphological analysis was carried on quenched sheared sample at room temperature after long time, and the results showed that it is similar to that of initial sample.

CONCLUSIONS

In this study, the rheological properties and morphology of the compatibilized and noncompatibilized PP/PET blends using SEBS-*g*-MA are investigated. It was observed that the storage modulus in plateau region increases by increasing the concentration of the compatibilizer. The morphological analysis for these compatibilized blends showed that a 3D agglomerated structure causes deviation from viscoelastic Palierne model. Similar results were observed in step strain experiments in linear region. Also, the experiments after cessation of various simple shear flows with higher shear stress values than G_p' have shown that the aggregated structure of dispersed particles was destroyed and replaced by an alignment in the flow direction for present imposed shear rates. This alignment was recovered by increasing the time interval between preshear and step strain experiment.

References

1. Galloway, J. A.; Montminy, M. D.; Macosko, C. W. Polymer 2002, 43, 4715.
2. Castro, M.; Carrot, C.; Prochazka, F. Polymer 2004, 45, 4095.
3. Van Hemelrijck, E.; Van Puyvelde, P.; Velankar, S.; Macosko, C. W.; Moldenaers, P. J Rheol 2004, 48, 143.
4. Van Puyvelde, P.; Velankar, S.; Moldenaers, P. Curr Opin Colloid Interface Sci 2001, 6, 457.
5. Lepers, J. C.; Favis, B. D.; Tabar, R. J. J Appl Polym Sci Part B: Polym Phys 1997, 35, 2271.
6. Papadopoulou, C. P.; Kalfoglou, N. K. Polymer 2000, 41, 2543.
7. Bousmina, M. Rheol Acta 1999, 38, 73.
8. Palierne, J. F. Rheol Acta 1990, 29, 204.
9. Goharpey, F.; Nazockdast, H.; Katbab, A. A. Polym Eng Sci 2005, 45, 84.
10. Bousmina, M.; Muller, R. Rheol Acta 1996, 35, 369.
11. Hobbs, S. Y.; Dekkers, M. E. J.; Watkins, V. H. Polymer 1988, 29, 1598.
12. Luzinov, I.; Pagnoulle, C.; Jerome, R. Polymer 2000, 41, 7099.
13. Wu, S. Polymer Interface and Adhesion; Marcel Dekker: New York, 1982.
14. Dealy, J. M.; Wissbrun, K. F. Melt Rheology and Its Role in Plastics Processing; Van Nostrand-Reinhold: New York, 1990.
15. Dealy, J. M.; Larson, R. G. Structure and Rheology of Molten Polymers; Hanser: Cincinnati, OH, 2006.
16. Iza, M.; Bousmina, M. J Rheol 2000, 44, 1363.
17. Soskey, P. R.; Winter, H. H. J Rheol 1984, 28, 625.
18. Ansari, M.; Haghtalab, A.; Semsarzadeh, M. A. Rheol Acta 2006, 45, 983.